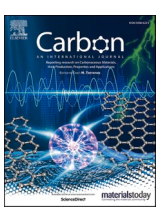
ELSEVIER

Contents lists available at ScienceDirect

Carbon

journal homepage: www.elsevier.com/locate/carbon



Polyamide-imide copolymer-derived carbon molecular sieve membranes for efficient hydrogen/carbon dioxide separation

Gaurav M. Iyer, Ching-En Ku, Chen Zhang

Department of Chemical and Biomolecular Engineering, University of Maryland, 4418 Stadium Drive, College Park, MD, 20742, United States

ARTICLE INFO

Keywords: Carbon molecular sieve membrane Microporous carbon Hollow fiber membrane Polyamide-imide Hydrogen separation

ABSTRACT

Carbon molecular sieve (CMS) membranes are emerging porous carbon membranes for chemical separation and purification. Polyamide-imide (PAI) copolymers have shown attractive separation performance for natural gas upgrading and organic solvent separations. However, PAIs are rarely used as precursors to derive CMS membranes. This work shows that CMS hollow fiber membranes made from a PAI (Torlon®) can provide highly competitive H2 permeability and H2/CO2 selectivity overcoming the 2008 Robeson upper bound under both single-gas and mixed-gas permeation. With imide and amide moieties, the PAI showed intermediate H2/CO2 separation performance between a polyimide (PI) and a polyaramid (PA). Interestingly, the trend was translated to the CMS membranes, i.e., the PAI-derived CMS membrane showed intermediate H₂/CO₂ separation performance between the PI-derived CMS membrane and PA-derived CMS membrane with an excellent balance of H₂ permeability and H₂/CO₂ selectivity. Sorption studies indicate that the PAI-derived CMS membrane had intermediate H₂ diffusivity and H₂/CO₂ diffusion selectivity, which was further attributed to its intermediate ultramicropore size. To our best knowledge, this was the first report of PAI-derived CMS hollow fiber membranes with competitive gas separation performance and the first investigation of the chemistry and pore structure of PAIderived porous carbon. This study also underscores the role of precursor backbone chemistry in tailoring CMS membrane properties, further suggesting that CMS membranes derived from copolymers comprising mixed backbone chemistry can give simultaneously attractive permeability and selectivity.

1. Introduction

Carbon molecular sieve (CMS) membranes are amorphous porous carbon membranes made by pyrolysis of polymer precursor membranes above their thermal decomposition temperatures. During pyrolysis, the aromatic polymer backbone decomposes to provide disorderly packed graphene sheets (micropores) with slit-like ultramicropores between neighboring aromatic strands. This unique pore structure allows CMS membranes to achieve high permeability and high selectivity overcoming the Robeson upper bounds [1,2]. The CMS membrane pore structure and gas separation performance are governed by several factors, among which are polymer precursor chemistry and pyrolysis conditions [3]. Several classes of polymer precursors have been studied including polyimides [4–10], polybenzimidazoles [11–13], polyaramids [14,15], polymers of intrinsic microporosity (PIMs) [16–19], polyvinylidene fluoride/chloride [20,21], and cellulose-based polymers [22–24].

Polyimides (PIs) represent the most widely studied class of CMS

membrane precursor [25-29]. This is likely because PIs are among the most commercially successful gas separation membrane materials [30]. Also, PIs exhibit large amount of carbon residue after pyrolysis. Many PIs have excellent solution processability and can be formed into hollow fibers by dry-jet/wet-quench spinning at room temperature, which allows the fabrication of scalable asymmetric or composite CMS hollow fiber membranes [28,29,31,32]. In addition, PI's well-understood structure-transport property relationship have allowed the fabrication of PI-derived CMS membranes with tunable separation performance. For example, the commercially available Matrimid® PI is arguably the most extensively reported CMS membrane precursor [27]. Work by Koros and co-workers in the past two decades showed that Matrimid®-derived CMS membranes can have controllable pore structure to give attractive separation performance for several gas pairs such as CO2/CH4 and C₂H₄/C₂H₆ [7,25]. The same group of researchers also developed highly permeable CMS membranes using PIs synthesized by bulky dianhydrides such as 4,4'-(Hexafluoroisopropylidene) diphthalic anhydride (6FDA) [5]. These highly permeable materials extended the spectrum of CMS

E-mail address: czhang71@umd.edu (C. Zhang).

^{*} Corresponding author.

membranes to separation of larger molecules such as C₃H₆/C₃H₈.

While PIs are broadly used for gas separation, polyaramids (PAs) are more commonly used for desalination [33-35] and rarely considered for gas separation [36]. This is due to strong hydrogen bonding between amide linkages in the PA backbone that gives low gas permeabilities under dry conditions [37]. PA-derived CMS membranes are much less studied than PI-derived CMS membranes. In a recent work [15], we developed CMS membranes using a solution-processable uncrosslinked polyaramid precursor (MTI) synthesized by m-phenylenediamine (MPD), terephthaloyl chloride (TPC), and isophthaloyl chloride (IPC). While the PA-derived CMS membrane showed ultra-high H₂/CO₂ ideal selectivity (up to 366), it had low H₂ permeability (9 Barrer). Separation of H2 from CO2 can recover H2 and capture CO2 from steam methane reforming products. High membrane H₂ permeability can help to reduce the required membrane area and hence the membrane separator cost. High membrane H₂/CO₂ selectivity can produce purer H₂ product. It would hence be attractive to achieve a balance between H2 permeability and H₂/CO₂ selectivity in CMS membranes for H₂/CO₂ separation.

Copolymer membranes are often made to provide balanced and sometimes synergistic separation performance unattainable in homopolymer membranes [38,39]. Fabrication of CMS membranes from copolymers comprising mixed backbone chemistry, however, is rarely reported. Polyamide-imides (PAIs) are copolymers consisting of both imide and amide backbones. Kosuri and Koros [40] fabricated defect-free asymmetric hollow fiber membranes using Torlon®, a commercially available PAI, which showed excellent plasticization resistance for purification of high-pressure natural gas. The same research group also synthesized a family of fluorinated PAIs with enhanced CO₂ and H₂S permeability [41]. More recently, Jang and co-workers [42] reported organic solvent reverse osmosis separation of liquid hydrocarbon mixtures in defect-free Torlon® hollow fiber membranes. Hosseini and Chung [11] made Torlon-derived CMS dense film membrane at 800 °C, which had moderate H2/CO2 ideal selectivity around 9. To our best knowledge, no CMS hollow fiber membranes have been derived from PAIs. Also, attractive gas separation performance has not been reported in PAI-derived CMS membranes.

In this work, we fabricated novel PAI-derived CMS hollow fiber membranes by pyrolysis of defect-free Torlon® PAI precursor hollow fiber membranes. The PAI-derived CMS membrane pyrolyzed at 925 °C showed a good balance of attractive H_2 permeability and outstanding H_2/CO_2 selectivity between the CMS membranes made from the MTI polyaramid and the Matrimid® polyimide at identical pyrolysis conditions. Sorption, diffusion, and pore structure of the novel PAI-derived CMS hollow fiber membranes were characterized and compared with the CMS membranes derived from the polyimide and polyaramid to gain an understanding on how precursor backbone chemistry affects CMS membrane pore structure and transport properties. The results suggest that pyrolysis of copolymers comprising mixed backbone chemistry can be an attractive strategy to fabricate CMS membranes with competitive separation performance.

2. Experimental section

2.1. Materials

Torlon® 4000 T-LV polyamide-imide was provided by Solvay Materials (Alpharetta, GA). Matrimid® 5218 polyimide was provided by Huntsman Corporation (Salt Lake City, UT). Tetrahydrofuran (THF, \geq 99.0 %, anhydrous), ethanol (\geq 99.5 %, anhydrous), and *N*-Methyl-2-pyrrolidone (NMP, anhydrous, 99.5 %) were obtained from Sigma Aldrich (St. Louis, MO). Hexane (\geq 98.5 %, mixture of isomers) and methanol (\geq 99.8 %) were obtained from VWR (Radnor, PA). *N*,*N*-dimethylacetamide (DMAc, \geq 99.8 %, anhydrous) was purchased from Fisher Scientific (Pittsburgh, PA). All chemicals were used with no purification. Pure gases (ultra-high purity) and gas mixtures (certified) were obtained from Airgas (Hyattsville, MD).

2.2. Fabrication of precursor dense films

Torlon® PAI dense films were fabricated using solution casting [15]. Torlon® PAI powders were dried under vacuum at 110 °C for 12 h before being dissolved (24 wt%) in DMAc to provide a polymer casting solution. The polymer solution was then cast on a borosilicate glass plate using a stainless-steel casting knife in a convection oven at 120 °C. After 12 h, the nascent film was peeled off from the borosilicate glass plate and soaked in methanol at ambient conditions for 12 h to remove the residual solvent. After being dried in a fume hood for 12 h, the film was further dried under vacuum at 210 °C for 24 h. Fabrication of Matrimid® PI dense films is described in the Supporting Information.

2.3. Fabrication of precursor hollow fiber membranes

Monolithic Torlon® PAI precursor hollow fiber membranes were made by dry-jet/wet-quench spinning using a customized hollow fiber spinning system (Fig. S1) [40]. Torlon® PAI powders were dried under vacuum at 110 °C for 12 h before preparing the spinning solution (Table 1). Tap water was used in the quench bath. The as-spun precursor hollow fibers were soaked in deionized water for 3 days, followed by soaking in methanol for 60 min and hexane for 60 min. After being dried in a fume hood for 12 h, the precursor hollow fibers were further dried under vacuum at 75 °C for 12 h. Fabrication of Matrimid® precursor hollow fiber membranes is described in the Supporting Information with spinning dope composition and spinning conditions shown in Table S1.

2.4. Fabrication of CMS membranes

CMS hollow fiber membranes and CMS dense film membranes were fabricated by pyrolysis in a 24-inch pyrolysis tube furnace (MTI Corporation, Richmond, CA). The precursor hollow fibers were placed on a stainless-steel mesh plate (McMaster Carr, Robbinsville, NJ) and loaded into a quartz tube (MTI Corporation, Richmond, CA) before being placed in the furnace. The precursor dense films were placed on a custom-made channeled quartz plate and loaded into a quartz tube before being placed in the furnace. Ultra-high purity argon was flown in the quartz tube at 0.2 L/min using a digital mass flow controller (MTI Corporation, Richmond, CA). The oxygen level inside the quartz tube was kept no higher than 5 ppm, which was measured by an oxygen sensor (Cambridge Sensotec, Saint Ives, UK). The pyrolysis heating protocol for each pyrolysis temperature (T_f) consisted of (1) Room temperature to 250 °C, 13.3 °C/min; (2) 250 °C to T_f·15, 3.85 °C/min; (3) T_f·15 to T_f, 0.25 °C/ min; (4) Dwelling at T_f for 2 h; (5) Natural cooling down to room temperature. Four PAI-derived CMS membranes were made at Tf of 675, 800, 925, and 1050 °C, which are codenamed PAI-675, PAI-800, PAI-925, and PAI-1050, respectively.

Table 1Spinning dope composition and hollow fiber spinning conditions for Torlon® PAI precursor hollow fiber membranes.

Spinning Conditions	Unit	Value
Dope composition	wt% Torlon®	34.0
	wt% NMP	47.2
	wt% THF	11.8
	wt% Ethanol	7.0
Spinning temperature	°C	50
Lab relative humidity	%	62
Quench bath temperature	°C	50
Dope/bore fluid flow rate	cm ³ /h	180/60
Bore fluid composition	NMP/H ₂ O	80/20
Air gap height	cm	22
Fiber take-up rate	m/min	32

2.5. Construction of CMS hollow fiber membrane modules

CMS hollow fiber membrane modules were made using stainless steel Swagelok® tubing and fittings following procedures described in literature [43]. Epoxy resin (3 M Scotch-Weld $^{\text{TM}}$ DP-100) was used for sealing.

2.6. Characterizations

Scanning electron microscopy (SEM) was done using a Tescan XEIA3 scanning electron microscope (Tescan, Warrendale, PA). Fourier transform infrared spectroscopy (FT-IR) was done using a ThermoNicolet Nexus 670 F T-IR spectrometer (Thermo Fisher Scientific, Waltham, MA). A Shimadzu TGA50 thermal gravimetric analyzer (Shimadzu, Columbia, MD) was used to measure the thermal decomposition temperature and carbon residual weight with a heating rate of 5 °C/min under continuous N₂ purge (50 cm³/min). Precursor polymer densities were measured using an analytical balance, which was equipped with a density kit (OHAUS, Parsippany, NJ) using isopropyl alcohol as the buoyant liquid. Wide-angle X-ray diffraction (WAXD) patterns were recorded using a Bruker D8 Advance Lynx powder diffractometer (LynxEye PSD detector, sealed tube, Cu Kα radiation with Ni β-filter). Raman spectroscopy was performed using the H-J-Y LabRam ARAMIS Confocal Raman Microscope equipped with a 532 nm laser. X-ray photoelectron spectroscopy (XPS) was performed using the Kratos AXIS Supra⁺ spectrometer. Determination of elemental composition and peak fitting of the C1s, N1s and O1s spectral scans were done in CasaXPS software. CO₂ physisorption (0 °C) was performed by an ASAP 2020Plus physisorption analyzer (Micromeritics, Norcross, GA). CMS dense films were degassed at 120 °C for 12 h prior to collection of CO₂ physisorption isotherms. A density functional theory (DFT) model (CO2, 0 °C, carbon slit pores) was used to obtain the CMS pore size distribution and cumulative pore volume.

2.7. Membrane permeation measurements

2.7.1. Single-gas permeation in Torlon® PAI precursor hollow fiber membranes

Single-gas permeation of CO_2 and N_2 was performed in the Torlon® PAI precursor hollow fiber using the constant pressure method [10] at ambient temperature (~20 °C). The feed was introduced to the hollow fiber shell side. The permeate flow rate was measured using a bubble flow meter.

2.7.2. Single-gas permeation in CMS hollow fiber membranes

Single-gas permeation measurements in the CMS hollow fiber membranes were performed at 35 $^{\circ}\mathrm{C}$ and 10 bar using the constant volume-variable pressure method [2]. The feed was introduced to the hollow fiber shell side and the permeate was collected from hollow fiber bore side. Hollow fiber membrane modules with at least two CMS hollow fibers were used for single-gas permeation tests. The permeation tests were allowed to proceed for at least 10 times of permeation time lag prior to flux measurement to ensure the permeation had reached steady state.

2.7.3. Mixed-gas permeation in CMS hollow fiber membranes

Mixed-gas permeation measurements (equimolar H_2/CO_2 mixture at 2 bar) were performed in the CMS hollow fiber membranes at 35 °C using a constant volume-variable pressure method. Composition of the permeate stream was measured using an Agilent 8890 gas chromatograph (Agilent Technologies, Santa Clara, CA). The stage cut was maintained below 1 % to avoid concentration polarization [10]. Gas chromatograph (GC) injections were taken continuously until a stable permeate composition was achieved.

2.8. Equilibrium sorption measurements in CMS membranes

Equilibrium sorption isotherms of H_2 and CO_2 were measured at 35 °C using an ASAP 2020Plus physisorption analyzer (Micromeritics, Norcross, GA) at pressure up to 1 bar. CMS dense films were degassed at 120 °C for 12 h prior to sorption isotherm collection. The H_2 sorption isotherms were fit using Henry's Law [44]. The CO_2 sorption isotherms were fit using the dual-mode sorption model [45].

3. Results and discussion

3.1. Formation of CMS membranes using PAI copolymer

Monolithic Torlon® PAI precursor hollow fiber membranes were fabricated using the dry-jet/wet-quench spinning process based on spinning dope composition and spinning parameters (Table 1) identified by Kosuri and Koros [40]. Scanning electron microscopy (SEM) shows that the PAI precursor hollow fibers (outer diameter $\sim 280 \mu m$) exhibited an asymmetric structure (Fig. 1A) with a porous substrate (Fig. 1B) having large and interconnected pores and a dense skin layer $(\sim 1 \mu m)$ on the outer surface (Fig. 1D). Slight densification was seen at the hollow fiber bore side (Fig. 1C) indicating premature phase separation by the bore fluid during fiber extrusion. The PAI precursor hollow fiber membranes showed CO2 permeance of 1.54 GPU and CO2/N2 ideal selectivity of 31.2 under single-gas CO₂/N₂ permeation at room temperature. The CO₂/N₂ ideal selectivity was within 90 % of the intrinsic value measured in thick Torlon® dense films [40], indicating that the PAI precursor hollow fiber membranes were defect-free [40]. Notably, although the lab relative humidity (62 %) during hollow fiber spinning was much higher than a previous work [42] (18 %), defect-free hollow fiber membranes were still obtained.

PAI-derived CMS hollow fiber membranes (outer diameter ~ 185 μm) were successfully made by pyrolysis of the defect-free Torlon® PAI precursor hollow fiber membranes at 675, 800, 925, and 1050 °C under continuous argon purge. Carbon molecular sieve hollow fiber membranes are traditionally made from precursor hollow fibers comprising polymers with high glass transition temperature (T_g) above 320 °C (e.g., polyimides, polybenzimidazoles). Pyrolysis of precursor hollow fibers comprising low- T_g polymers (e.g., polyvinylidene fluoride) can lead to structural deformation in CMS hollow fiber membranes [20]. Although the Torlon® PAI had lower $T_{\rm g}$ (273 °C) [40] than polyimides and polybenzimidazoles, CMS hollow fiber membranes were successfully formed without any structural deformation (Fig. 1E and Fig. S2). Without pre-treatments [28], pore collapse and wall densification are known to occur [7] in precursor hollow fibers during pyrolysis. The PAI precursor hollow fibers underwent pore collapse during pyrolysis and hence the PAI-derived CMS hollow fiber membranes had totally densified wall of 51 µm with few macrovoids (Fig. 1F-H). The totally densified wall allowed for unambiguous determination of the CMS membrane's separation layer thickness (51 μm).

3.2. Gas separation performance of PAI-derived CMS membranes

We carried out single-gas (He, H_2 , CO_2 , N_2 , and CH_4) permeation in the PAI-derived CMS hollow fiber membranes at 10 bar and 35 °C. As the pyrolysis temperature increased, gas permeabilities (Fig. 2A and Table S2) and permeances (Fig. S3) were reduced with increased H_2/N_2 , H_2/CO_2 , H_2/CO_2 , and H_2/H_2 ideal selectivities (Fig. 2B). It should be noted that CH_4 permeation can only be reliably measured in PAI-675. Also, only He and H_2 permeabilities can be reliably measured in PAI-1050. The H_2/CO_2 separation performance of the PAI-derived CMS membranes are shown in Fig. 2C. The PAI precursor shows H_2/CO_2 separation performance below the 2008 Robeson upper bound [1] with H_2 permeability of 4.4 Barrer and H_2/CO_2 ideal selectivity of 5.3. The PAI-675 CMS membrane showed over 235 times higher H_2 permeability (1034 Barrer) and slightly lower H_2/CO_2 ideal selectivity (4.9)

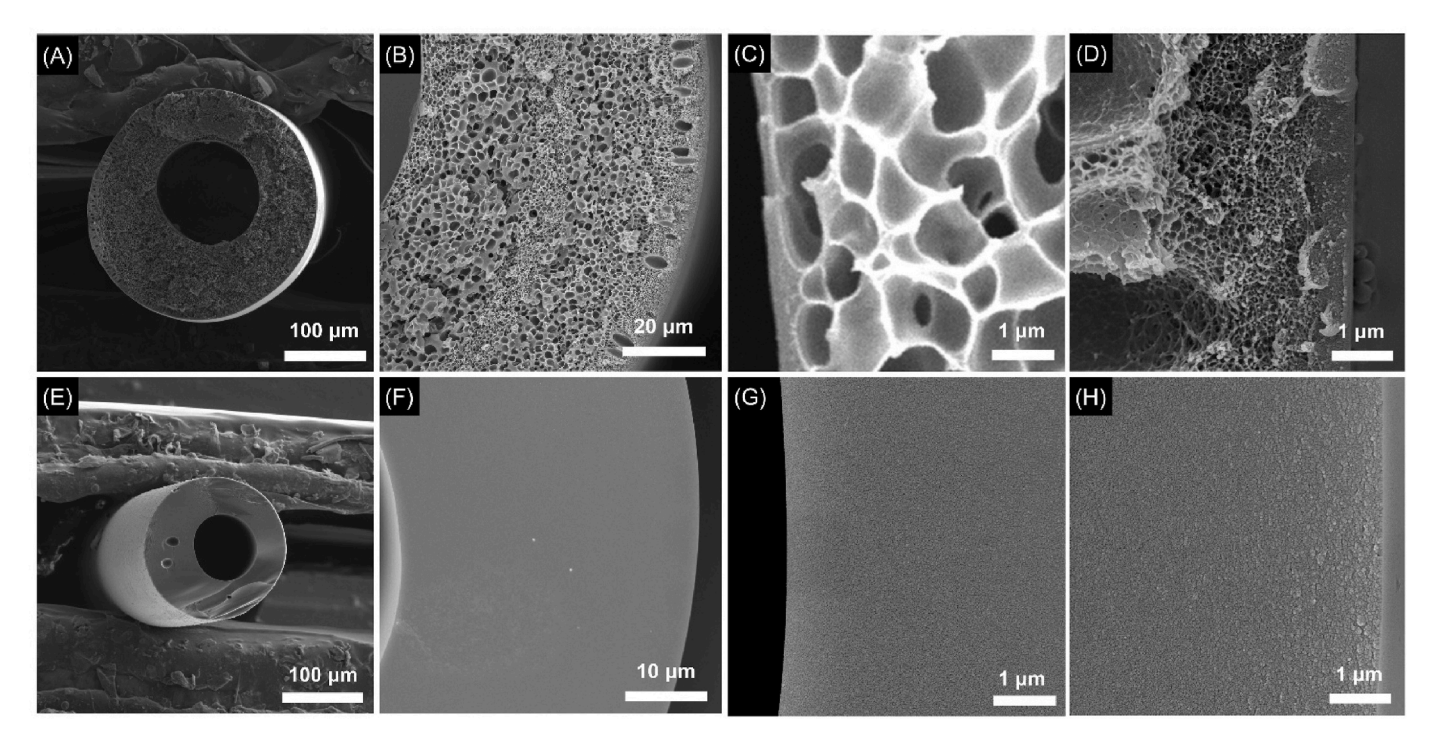


Fig. 1. SEM images of defect-free Torlon® PAI precursor hollow fiber membranes and PAI-derived CMS hollow fiber membranes. (A) Precursor hollow fiber overview; (B) Precursor hollow fiber wall; (C) Precursor hollow fiber inner bore; (D) Precursor hollow fiber outer surface; (E) CMS hollow fiber overview; (F) CMS hollow fiber wall; (G) CMS hollow fiber inner bore; (H) CMS hollow fiber outer surface. (A colour version of this figure can be viewed online.)

than the PAI precursor. As the pyrolysis temperature increased to 800 and 925 °C, the $\rm H_2$ permeability dropped with increased $\rm H_2/CO_2$ ideal selectivity. The trend was seen in several polyimide-derived CMS membranes, which was believed to be due to refined ultramicropores at higher pyrolysis temperatures [2,25]. Among the studied PAI-derived CMS membranes, the PAI-925 CMS membrane showed optimal $\rm H_2/CO_2$ separation performance well above the 2008 Robeson upper bound with 7-fold higher $\rm H_2/CO_2$ ideal selectivity (94) than the PAI precursor.

Similar enhancements in separation performance were seen for the He/CO₂ pair (Fig. 2D), in which the PAI-925 CMS membrane showed 3fold higher He permeability (19.9 Barrer) and 8-fold higher He/CO2 ideal selectivity (57) than the PAI precursor. While He/CO2 permeation results are much less reported than the H2/CO2 pair, it is an important separation for helium extraction from natural gas [46]. Comparing the results shown in Fig. 2C and D indicate that it is more challenging for CMS membranes to overcome the Robeson upper bound for the He/CO₂ pair than for the H₂/CO₂ pair. The CO₂ permeation flux in the PAI-1050 CMS membrane was below the detection limit of the permeation system. Although the PAI-1050 CMS membrane likely had even higher H₂/CO₂ and He/CO2 ideal selectivities than the PAI-925 CMS membrane, it had lower H₂ and He permeabilities. While the PAI-675 CMS membrane had low H2/CO2 and He/CO2 ideal selectivities, it showed a good balance of attractive H2 permeability (1034 Barrer) and H2/CH4 ideal selectivity (577).

In addition to single-gas H_2/CO_2 permeation, we performed H_2/CO_2 mixed-gas permeation measurements (Fig. 2C) in the PAI-925 CMS membrane using an equimolar H_2/CO_2 mixture at 2 bar and 35 °C. It should be noted that H_2/CO_2 mixed-gas permeation measurements were not performed in the PAI-675 CMS membrane and PAI-800 CMS membrane because their H_2/CO_2 separation performance was less attractive. The mixed-gas H_2 permeability (16 Barrer) and H_2/CO_2 separation factor (57) of the PAI-925 CMS membrane were lower than the H_2 permeability and H_2/CO_2 ideal selectivity measured under single-gas permeation likely due to competitive sorption effects from the highly condensable CO_2 . Similar reductions in H_2 permeability and H_2/CO_2

separation factor under mixture permeation were observed in CMS membranes derived from other polymer precursors [12,18]. Nevertheless, the $\rm H_2/CO_2$ mixed-gas separation performance of the PAI-925 CMS membrane was still above the 2008 Robeson upper bound.

To further understand CMS membrane formation using copolymers comprising mixed backbones, we compared the PAI-925 CMS membrane with CMS membranes derived from polyaramid (MTI) and polyimide (Matrimid®) at identical pyrolysis conditions at 925 °C, which are codenamed PA-925 CMS (Fig. S4) and PI-925 CMS (Fig. S5), respectively. The three CMS hollow fiber membranes showed comparable mechanical flexibility (Fig. S6). The H₂/CO₂ permeation results of the PA-925 CMS membrane were reported in our previous work [15]. Defect-free Matrimid® polyimide precursor hollow fibers were spun and pyrolyzed at 925 °C to provide the PI-925 CMS membrane (Supporting Information). The chemical structure and FT-IR spectra of the Matrimid® polyimide, Torlon® polyamide-imide, and MTI polyaramid are shown in Fig. 3A and B, respectively. The three polymer precursors are all uncrosslinked linear polymers with rigid aromatic backbones and without bulky side groups. The characteristic IR stretching peak at ~3300 cm⁻¹ corresponding to hydrogen-bonded N–H stretching vibration is the strongest in PA, relatively weaker in the PAI, and absent in the PI [47]. Additionally, absence of the characteristic peak at ~3446 cm⁻¹ (free N-H stretching vibrations) indicates that all N-H groups are hydrogen-bonded in the polyaramid and polyamide-imide precursors (Fig. S7) [40]. Comprising both imide and amide backbones, the polyamide-imide showed intermediate density (PA: 1.37 g/cm³; PAI: 1.36 g/cm³; PI: 1.25 g/cm³), d-spacing (PA: 3.86 Å; PAI: 4.31 Å; PI: 6.22 Å), and thermal decomposition temperature (PA: 400 °C; PAI: 420 °C; PI: 475 °C) with comparable carbon residual (\sim 50–55 %) at 950 °C (Fig. 3C) [15].

The PAI also showed intermediate H_2 permeability and H_2/CO_2 ideal selectivity between the PA and PI (Fig. 4A). Interestingly, the trend was translated into the CMS membranes, i.e., the PAI-925 CMS membrane showed intermediate H_2 permeability and H_2/CO_2 ideal selectivity between the PA-925 CMS membrane and PI-925 CMS membrane. The PA-925 CMS membrane had ultra-high H_2/CO_2 ideal selectivity (366),

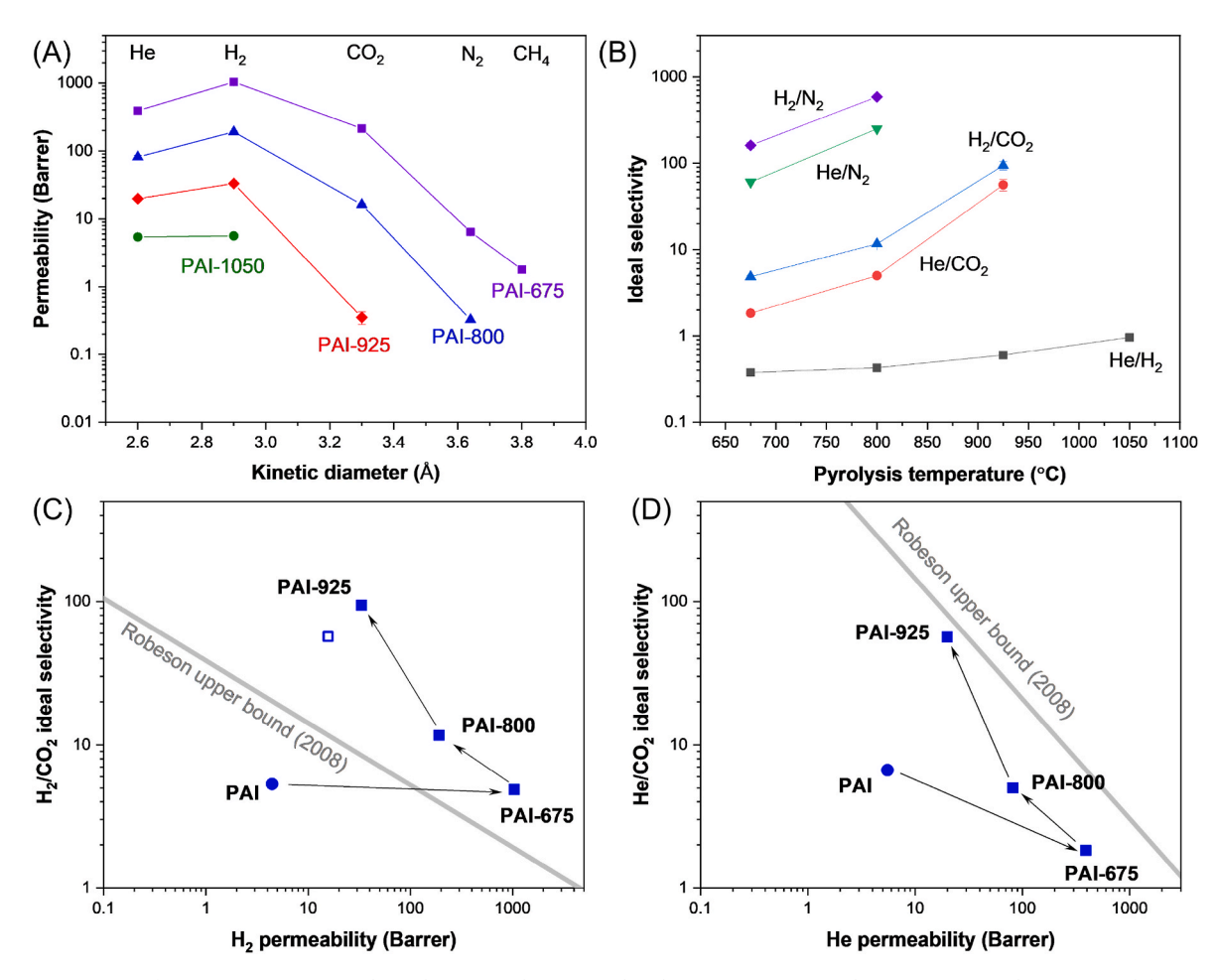


Fig. 2. Gas separation performance (35 $^{\circ}$ C) in PAI-derived CMS membranes pyrolyzed at 675, 800, 925, and 1050 $^{\circ}$ C. (A) Single-gas permeabilities; (B) ideal selectivities; (C) H₂/CO₂ separation performance; (D) He/CO₂ separation performance. (Solid symbols: single-gas permeation results; hollow symbols: mixed-gas permeation results).

however, had low $\rm H_2$ permeability of 9 Barrer [15]. The PI-925 CMS membrane had much higher $\rm H_2$ permeability (117 Barrer) yet with unattractive $\rm H_2/CO_2$ ideal selectivity (12.7). In comparison, the PAI-925 CMS membrane showed a good balance of attractive $\rm H_2$ permeability and $\rm H_2/CO_2$ ideal selectivity. Similar trend was observed for the $\rm He/CO_2$ pair, i.e., the PAI-925 CMS membrane showing intermediate $\rm He/CO_2$ separation performance with a good balance between $\rm He$ permeability and $\rm He/CO_2$ ideal selectivity (Fig. 4B).

The H₂/CO₂ separation performance of the PAI-925 CMS membrane remains competitive if compared with CMS membranes derived from a broader range of precursors (Fig. S8). For example, it shows competitive H₂/CO₂ separation performance with CMS membranes made from polybenzimidazole at comparable pyrolysis conditions, a rigid flameretardant polymer with much higher Tg (427 °C) than the Torlon® PAI. To our best knowledge, this was the first time that competitive gas separation performance was reported in PAI-derived CMS membranes. Although Matrimid®-derived CMS membranes can give ultra-high H₂/ CH₄ selectivity above 40,000 and CO₂/CH₄ selectivity above 3600 [2], it is not competitive with the PAI-derived CMS membrane and PA-derived CMS membrane for H₂/CO₂ and He/CO₂ separation. The results shown in Fig. 4 had three implications to the fundamental understanding of structure-property relationships in CMS membranes. First, precursor backbone chemistry is crucial to determine the separation performance of CMS membranes. Second, differences in precursor transport properties may be amplified in the derived CMS membranes. For example, the PAI precursor had 1.2 times higher H₂/CO₂ ideal selectivity than the PI precursor, whereas the PAI-925 CMS membrane had almost 7 times higher ${\rm H_2/CO_2}$ ideal selectivity than the PI-925 CMS membrane. Third, pyrolysis of copolymer precursors with mixed backbone chemistry can provide CMS membranes with simultaneously attractive permeability and selectivity.

3.3. Sorption and diffusion in CMS membranes

We measured H_2 and CO_2 sorption isotherms (Fig. 5A&B) in the PAI-925 CMS membrane at 35 °C. Henry's law was used to fit the H_2 sorption isotherm, whereas the dual-mode sorption model [45] was used to fit the CO_2 sorption isotherm to obtain the sorption parameters (Table S3). The sorption parameters allowed us to calculate H_2 and CO_2 sorption coefficients (Table S4) and H_2/CO_2 sorption selectivity (Fig. 5C) in the PAI-925 CMS membrane. Based on the single-gas H_2/CO_2 permeation results (Fig. 2A) and the sorption-diffusion model [48], H_2 and CO_2 diffusivity (Table S4) and H_2/CO_2 diffusion selectivity (Fig. 5C) in the PAI-925 CMS membrane were obtained. The PAI-925 CMS membrane had outstanding H_2/CO_2 diffusion selectivity \sim 1600. Due to much higher condensability, CO_2 sorbs much more strongly than H_2 and the PAI-925 CMS membrane had very low H_2/CO_2 sorption selectivity \sim 0.05.

The $\rm H_2$ and $\rm CO_2$ sorption properties of the PAI-925 CMS membrane were compared with the PI-925 CMS membrane and the PA-925 CMS membrane. All CMS membranes had similar $\rm H_2$ sorption coefficients (Table S4). The PAI-925 CMS membrane had comparable $\rm H_2/CO_2$ sorption selectivity with the PI-925 CMS membrane (\sim 0.06), which was lower than the PA-925 CMS membrane (\sim 0.11). The $\rm H_2/CO_2$ diffusion

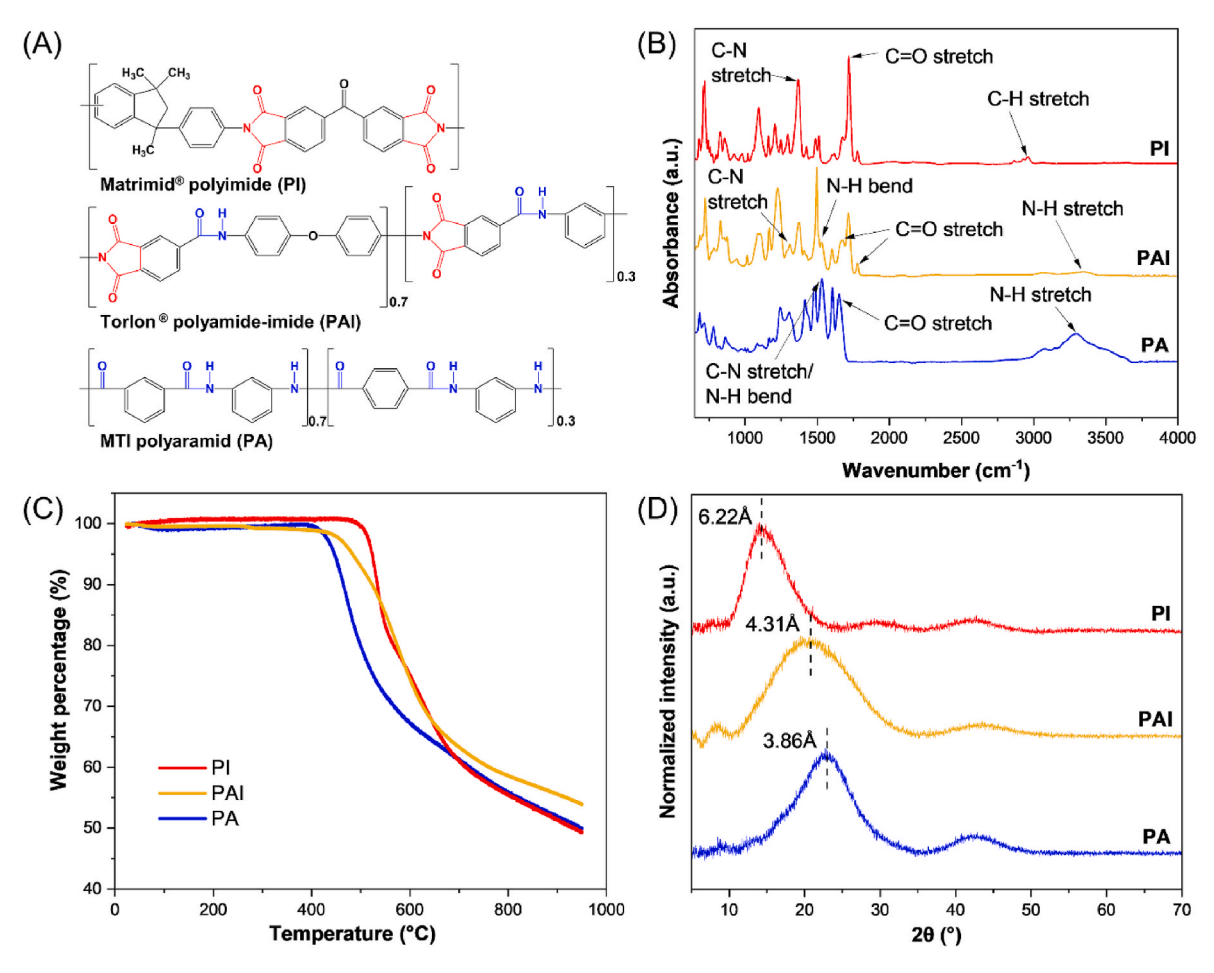


Fig. 3. (A) Chemical structures of polymer precursors; (B) FT-IR spectra of polymer precursors indicating characteristic peaks; (C) TGA weight loss profiles of polymer precursors up to 950 °C (N₂ purge); (D) WAXD spectra of polymer precursors indicating d-spacing. (A colour version of this figure can be viewed online.)

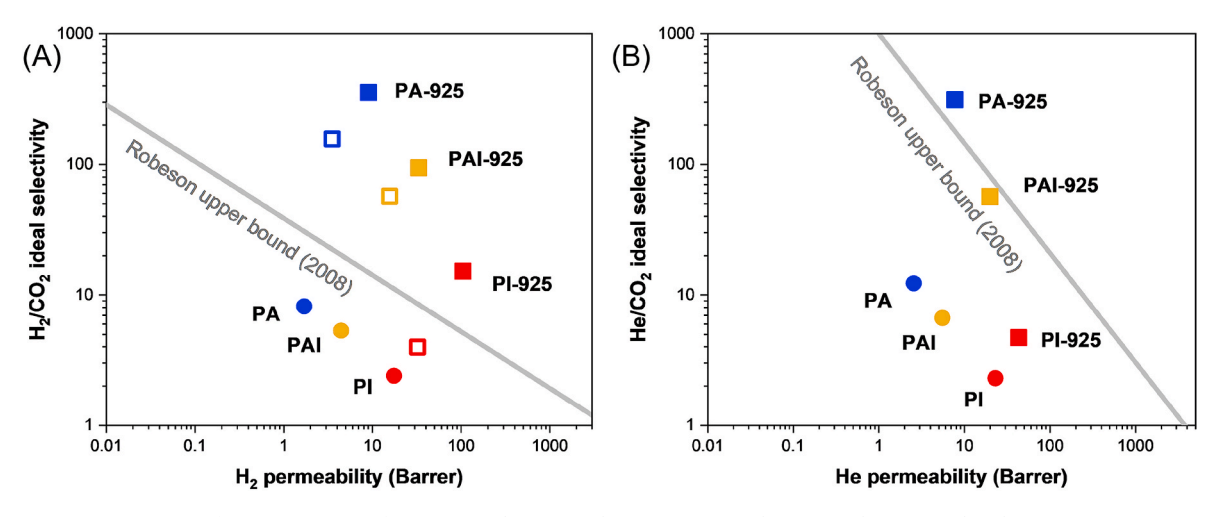


Fig. 4. (A) H_2/CO_2 separation performance (35 °C) of precursor polymer membranes [11,22] and CMS membranes pyrolyzed at 925 °C. (B) He/CO_2 separation performance (35 °C) of precursor polymer membranes [9,40] and CMS membranes pyrolyzed at 925 °C. (Solid symbols: single-gas permeation results; hollow symbols: mixed-gas permeation results; squares: permeation results of CMS membranes; circles: permeation results of precursor polymer membranes.) The H_2/CO_2 permeation results of the PA-925 CMS membrane were reported in Ref. [14]. (A colour version of this figure can be viewed online.)

selectivity of the PI-925 CMS membrane was only 204, which was responsible for its unattractive $\rm H_2/CO_2$ ideal selectivity (Fig. 4A). The ultra-high $\rm H_2/CO_2$ ideal selectivity of the PA-925 CMS membrane can be attributed to its $\rm H_2/CO_2$ diffusion selectivity of 3000 [15]. Notably, the PAI-925 CMS membrane had intermediate $\rm H_2$ diffusivity and $\rm H_2/CO_2$

diffusion selectivity between the PI-925 CMS membrane and the PA-925 CMS membrane, which was responsible for its good balance of $\rm H_2$ permeability and $\rm H_2/CO_2$ selectivity.

The $\rm H_2/CO_2$ diffusion selectivity reflects the CMS membrane ultramicropore's capability to differentiate $\rm H_2$ and $\rm CO_2$ molecules based on

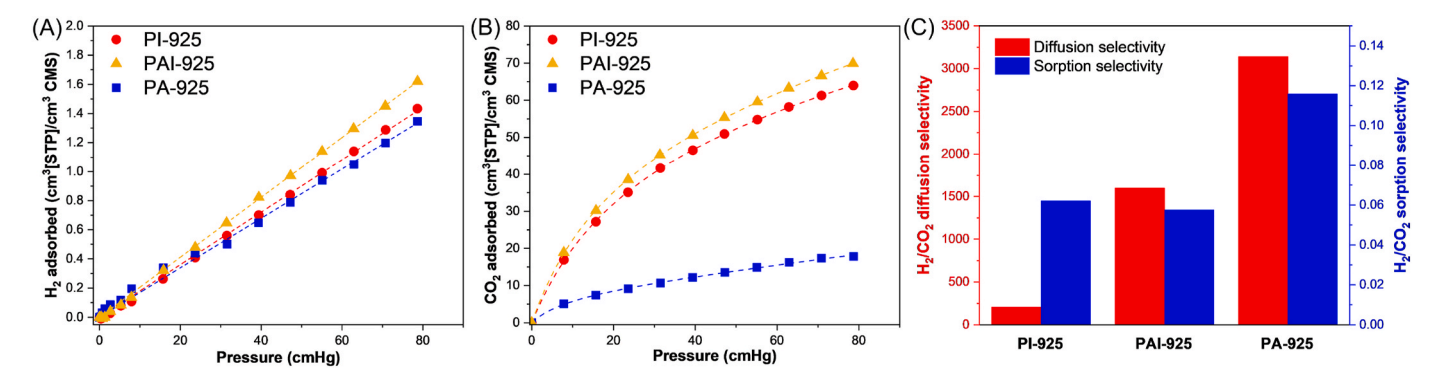


Fig. 5. (A) H_2 sorption isotherms and (B) CO_2 sorption isotherms (35 °C) in CMS membranes pyrolyzed at 925 °C; (C) H_2/CO_2 diffusion selectivity and H_2/CO_2 sorption selectivity in CMS membranes pyrolyzed at 925 °C. The H_2 and CO_2 sorption isotherms of the PA-925 CMS membrane were reported in Ref. [14]. (A colour version of this figure can be viewed online.)

their kinetic diameter difference (2.9 vs 3.3 Å). Since the PAI-925 CMS membrane had intermediate H₂/CO₂ diffusion selectivity, we hypothesize that it had intermediate ultramicropore size between the PI-925 CMS membrane and PA-925 CMS membrane. While moieties other than amide or imide can be found in the polymer backbones (e.g., ketone in the PI and ether in the PAI), it was apparent that the precursor average d-spacing (Fig. 3D) was dominated by hydrogen bonding provided by the amide moiety, i.e., PI (6.22 Å) > PAI (4.31 Å) > PA (3.86 Å). With strong hydrogen bonding provided by the highly concentrated amide moieties, the PA had closely packed chains and the smallest d-spacing. With mixed amide and imide backbone chemistry and weaker hydrogen bonding (Fig. 3B and Fig. S7), the PAI precursor had less closely packed chains and larger d-spacing than the PA precursor. Without amide moiety and hydrogen bonding, the PI precursor had the least closely packed chains and the largest d-spacing. Polymer precursors with closely packed chains can provide closely packed aromatic strands and graphitic plates during pyrolysis to give CMS membranes with small ultramicropores. Therefore, the intermediate ultramicropore size of the PAI-925 CMS membrane can be attributed to the intermediate d-spacing in the PAI precursor.

3.4. Pore structure characterization of CMS membranes

To support the hypothesis that the PAI-derived CMS membrane had intermediate ultramicropore size, we characterized the pore structure of the CMS membranes. Physisorption of CO_2 at 0 $^{\circ}C$ is widely used to examine CMS membrane pore structure. The CO_2 sorption isotherms (Fig. 6A) were fitted with a DFT model (0 $^{\circ}C$, carbon slit pores) to obtain the pore size distribution curves (Fig. 6B) and cumulative pore volume (Fig. 6C). The PAI-925 CMS membrane had similar pore volume to the PI-925 CMS membrane, which were both much larger than the PA-925

CMS membrane. Notably, no appreciable differences in pore size were seen in the three CMS membranes.

While CO_2 physisorption is broadly used to study the pore structure of nanoporous carbon [2,49], we believe it is not useful to characterize highly refined ultramicropores smaller than 3.0 Å to obtain the crucial pore structure knowledge needed to evaluate CMS membranes for H_2/CO_2 separations. It cannot characterize ultramicropores smaller than 3.3 Å due to exclusion of the CO_2 probe molecule (kinetic diameter 3.3 Å) [15]. In fact, the DFT model can only calculate pores larger than 3.6 Å if CO_2 sorption isotherms are used. As the pyrolysis temperature of the PAI-derived CMS membrane increased, the He/H_2 ideal selectivity was enhanced (Fig. 2B). This can be attributed to refining of the ultramicropores between the kinetic diameters of He (2.6 Å) and H_2 (2.9 Å), which is evidence that ultramicropores smaller than 3.0 Å existed. These sub-3.0 Å ultramicropores possibly played important roles in H_2/CO_2 separation in the CMS membranes.

Since CO_2 physisorption was not useful, was carried out X-ray photoelectron spectroscopy (XPS) to characterize the CMS membrane pore structure. The results show that all three CMS membranes contained carbon, nitrogen, and oxygen (Fig. 7A–C and Fig. S9). High-resolution C1s spectra were obtained to quantify the sp^3/sp^2 carbon ratio in the CMS membranes (Fig. 7D–F). The C1s spectra were deconvoluted into three peaks corresponding to sp^2 C (284 eV), sp^3 C (286 eV) and C–O functionalities (290 eV) [50]. The ratio of sp^3/sp^2 carbon was evaluated using the ratio of the respective peak areas in the C1s spectra [8,24]. The sp^3/sp^2 carbon ratio is indicative of the level of disorder in the amorphous graphitic structure of the CMS membranes, i.e., smaller sp^3/sp^2 carbon ratio suggests a more ordered graphitic structure and hence smaller CMS membrane inter-plate spacing and ultramicropore size. The sp^3/sp^2 carbon ratio of the three CMS membranes had the following order: PI-925 sp^2 PAI-925. The finding thus supports

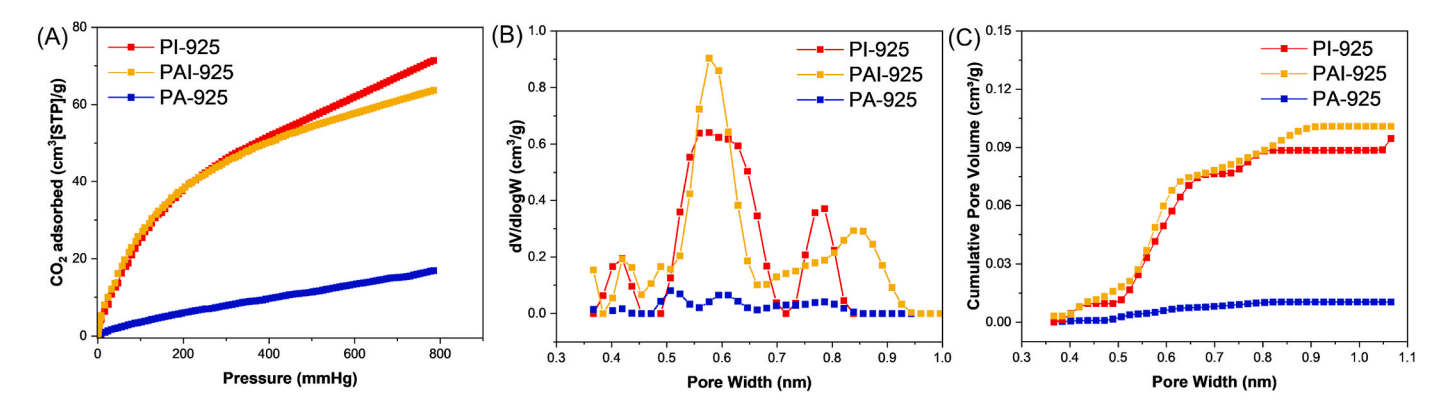


Fig. 6. Characterizing the CMS membrane pore structure using CO_2 physisorption at 0 °C. (A) CO_2 physisorption isotherms; (B) Pore size distribution curves; (C) Cumulative pore volume. The CO_2 physisorption results of the PA-925 CMS membrane were reported in Ref. [14]. (1 cm³ [STP]/g = 0.0446 mmol/g).

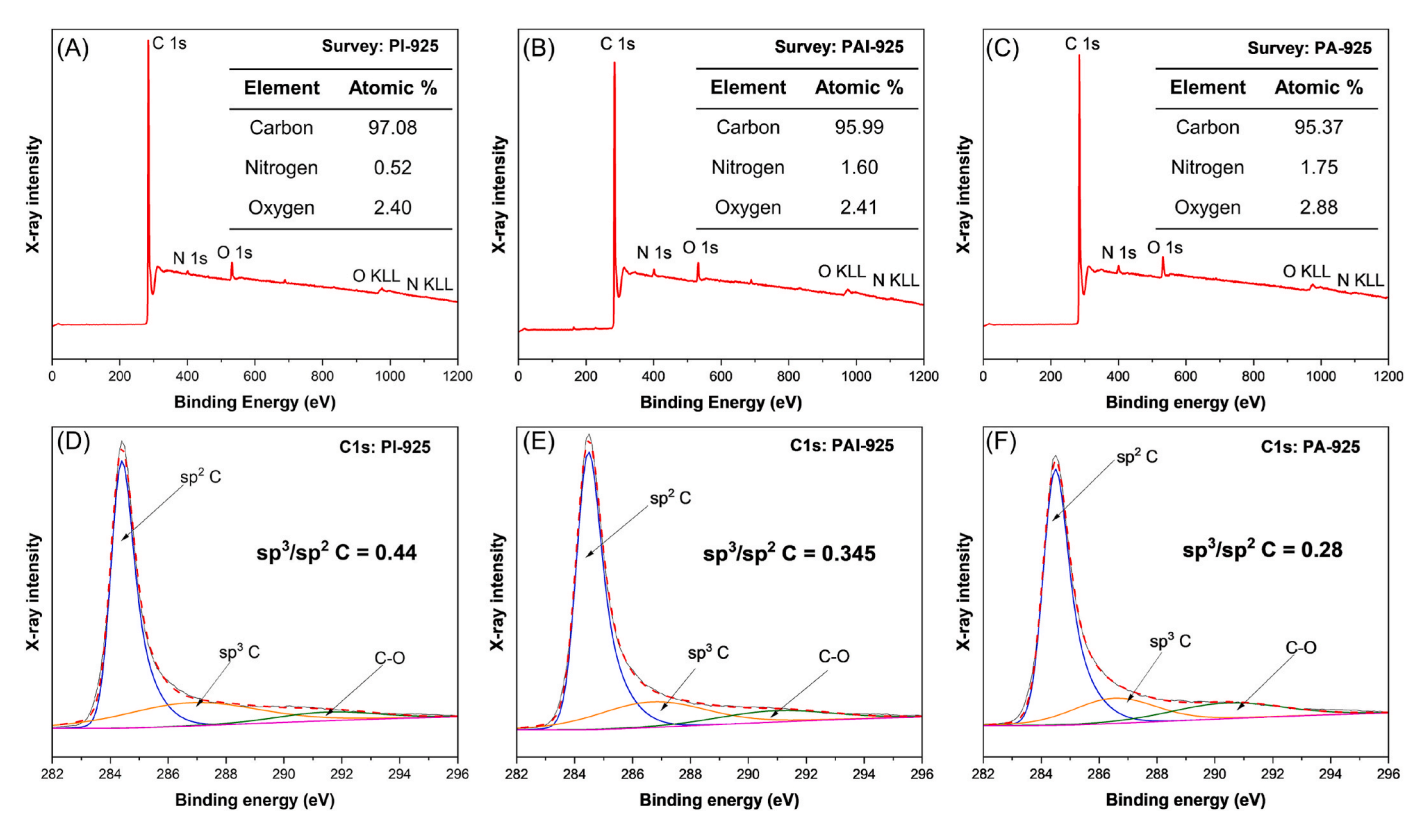


Fig. 7. (A–C) XPS survey spectra and (D–F) high-resolution C1s spectra of CMS membranes. The insets in (A–C) indicate the elemental composition of each CMS membrane. (A colour version of this figure can be viewed online.)

the hypothesis that the PAI-derived CMS membrane has intermediate ultramicropore size.

In addition to pore structure characterization, XPS results are useful to understand the role of sorption in CMS membranes. The CMS membrane nitrogen weight percentage (PA-925 [1.75 %] > PAI-925 [1.6 %] > PI-925 [0.52 %]) follows the same trend of CO $_2$ Langmuir affinity constants (PA-925 [0.105 cmHg $^{-1}$] > PAI-925 [0.047 cmHg $^{-1}$] > PI-925 [0.040 cmHg $^{-1}$], Table S3). The higher nitrogen weight percentage possibly gave higher surface heterogeneity of CMS membranes and hence stronger CO $_2$ adsorption [8]. The stronger CO $_2$ adsorption, however, is offset by much slower CO $_2$ diffusion, and H $_2$ /CO $_2$ separation in the CMS membranes studied in this work is governed by diffusion selectivity.

To complement the XPS analysis, we performed WAXD (Figure S10) and Raman spectroscopy (Fig. 8) to further investigate the CMS membrane pore structure. The PAI-925 CMS membrane and PA-925 CMS

membrane showed similar d-spacing (3.61 Å), which were both smaller than the PI-925 CMS membrane (3.82 Å). While WAXD results are generally valuable to understand the pore structure of CMS materials, several previous studies [2,13] showed that WAXD had limitations to characterize CMS membranes with highly refined ultramicropores. Two characteristic bands commonly observed for amorphous carbonaceous materials – the D band (\sim 1350 cm⁻¹) and G band (\sim 1590 cm⁻¹) were seen in the Raman spectra of all three CMS membranes. The D band was related to the A_{1g}-symmetry vibrational mode of structural defects, indicating presence of disorder in the carbon structure. The G band was related to the $E_{2\sigma}$ -symmetry mode of the aromatic sp²-carbon and linear chains corresponding to C=C in-plane stretching in graphitic carbon materials. With increasing degree of disorder and presence of oxygenated functionalities, secondary peaks appear in the D band. Therefore, each Raman spectrum was decoupled using 5 Gaussian peaks - D1, D2, D3, D4, G to fit the experimental data [23]. The D1 peak (\sim 1350 cm⁻¹)

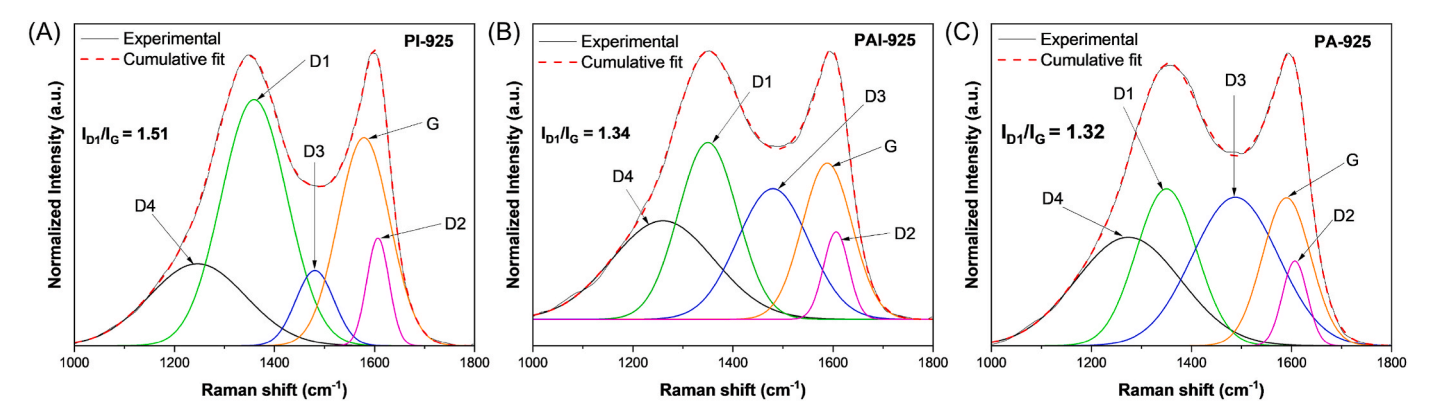


Fig. 8. Raman spectra of (A) PI-925 CMS membrane; (B) PAI-925 CMS membrane; (C) PA-925 CMS membrane. The Raman spectra of the PA-925 CMS membrane was reported in Ref. [14]. (A colour version of this figure can be viewed online.)

was associated with the basal plane defects in the graphitic structure. The $I_{\rm D1}/I_{\rm G}$ ratio [23] can be used as a measure of the concentration of $\rm sp^2$ carbon, i.e., lower $I_{\rm D1}/I_{\rm G}$ ratio indicates higher concentration of $\rm sp^2$ carbon and smaller ultramicropores. The $I_{\rm D1}/I_{\rm G}$ ratio of the three CMS membranes had the following order: PI-925 > PAI-925 > PA-925. The finding is hence consistent with the results of XPS and supports the hypothesis that the PAI-derived CMS membrane has intermediate ultramicropore size.

4. Conclusions

To summarize, we developed novel carbon molecular sieve (CMS) hollow fiber membranes for H2/CO2 and He/CO2 separation using a polyamide-imide (PAI) copolymer precursor. The PAI-derived CMS hollow fiber membranes pyrolyzed at 925 °C showed a good balance of $\rm H_2$ permeability (33 Barrer) and $\rm H_2/CO_2$ ideal selectivity (94) well above the 2008 Robeson upper bound under single-gas permeation. Under mixed-gas permeation, the membrane remained above the 2008 Robeson upper bound with attractive H₂ permeability (16 Barrer) and H₂/CO₂ separation factor (57). The PAI-derived CMS membrane was compared with CMS membranes derived from polyimide (PI) and polvaramid (PA) precursors at identical pyrolysis conditions at 925 °C. The PAI had intermediate H₂ permeability and H₂/CO₂ selectivity between the PI and PA. The trend was translated into the CMS membranes, with the PAI-derived CMS membrane showing intermediate H₂ permeability and H₂/CO₂ selectivity between the PI-derived CMS membrane and the PA-derived CMS membrane. Sorption studies suggest that it was because the PAI-derived CMS membrane had intermediate H₂ diffusivity and H₂/ CO2 diffusion selectivity, which was attributed to its intermediate ultramicropore size.

To our best knowledge, this is the first study of PAI-derived CMS hollow fiber membranes showing attractive separation performance. It is also the first systematic investigation of CMS membranes derived from copolymer precursor comprising mixed backbone chemistry via a comparison with CMS membranes derived from precursors comprising the individual backbones. The findings of this work have three implications to the fundamental understanding of structure-property relationships in CMS membranes. First, precursor backbone chemistry is crucial to determine the separation performance of CMS membranes. Second, differences in precursor transport properties may be amplified in the derived CMS membranes. Third, pyrolysis of copolymers with mixed backbone chemistry can be used as a strategy to develop CMS membranes with simultaneously attractive permeability and selectivity.

CRediT authorship contribution statement

Gaurav M. Iyer: Methodology, Investigation, Validation, Formal analysis, Writing – original draft, Writing – review & editing. **Ching-En Ku:** Investigation, Validation, Formal analysis, Writing – original draft, Writing – review & editing. **Chen Zhang:** Conceptualization, Funding acquisition, Supervision, Project administration, Writing – review & editing.

Declaration of competing interest

The authors declare that they have no known competing financial interests or personal relationships that could have appeared to influence the work reported in this paper.

Acknowledgment

Acknowledgment is made to the donors of the American Chemical Society Petroleum Research Fund for partial support of this research (Award No. 65081-DNI10). The authors thank additional funding from the National Science Foundation (CBET Award No. 1928325). The authors acknowledge Solvay Materials for kindly giving Torlon® polymer

samples and the Huntsman Corporation for kindly giving Matrimid® polymer samples. The authors thank Lu Liu for fabricating Matrimid® precursor hollow fibers. The authors also thank Professor Dongxia Liu for providing access to the TGA instrument and Dr. Karen Gaskell from the University of Maryland Surface Analysis Center for helping with XPS measurements. The authors also acknowledge the support of the Maryland NanoCenter and the AIMLab.

Appendix A. Supplementary data

Supplementary data to this article can be found online at https://doi.org/10.1016/j.carbon.2023.118598.

References

- L.M. Robeson, The upper bound revisited, J. Membr. Sci. 320 (1–2) (2008) 390–400.
- [2] C. Zhang, W.J. Koros, Ultraselective carbon molecular sieve membranes with tailored synergistic sorption selective properties, Adv. Mater. 29 (33) (2017), 1701631.
- [3] M. Kiyono, P.J. Williams, W.J. Koros, Effect of polymer precursors on carbon molecular sieve structure and separation performance properties, Carbon 48 (15) (2010) 4432–4441.
- [4] H. Hatori, H. Takagi, Y. Yamada, Gas separation properties of molecular sieving carbon membranes with nanopore channels, Carbon 42 (5) (2004) 1169–1173.
- [5] S. Fu, E.S. Sanders, S.S. Kulkarni, W.J. Koros, Carbon molecular sieve membrane structure–property relationships for four novel 6FDA based polyimide precursors, J. Membr. Sci. 487 (2015) 60–73.
- [6] X. Ning, W.J. Koros, Carbon molecular sieve membranes derived from Matrimid® polyimide for nitrogen/methane separation, Carbon 66 (2014) 511–522.
- [7] L. Xu, M. Rungta, W.J. Koros, Matrimid® derived carbon molecular sieve hollow fiber membranes for ethylene/ethane separation, J. Membr. Sci. 380 (1–2) (2011) 138–147.
- [8] W. Qiu, J.E. Leisen, Z. Liu, W. Quan, W.J. Koros, Key features of polyimide-derived carbon molecular sieves, Angew. Chem. Int. Ed. 60 (41) (2021) 22322–22331.
- [9] X. Ma, Y.S. Lin, X. Wei, J. Kniep, Ultrathin carbon molecular sieve membrane for propylene/propane separation, AIChE J. 62 (2) (2016) 491–499.
- [10] C. Zhang, G.B. Wenz, P.J. Williams, J.M. Mayne, G. Liu, W.J. Koros, Purification of aggressive supercritical natural gas using carbon molecular sieve hollow fiber membranes, Ind. Eng. Chem. Res. 56 (37) (2017) 10482–10490.
- [11] S.S. Hosseini, T.S. Chung, Carbon membranes from blends of PBI and polyimides for N2/CH4 and CO2/CH4 separation and hydrogen purification, J. Membr. Sci. 328 (1) (2009) 174–185.
- [12] M. Omidvar, H. Nguyen, H. Liang, C.M. Doherty, A.J. Hill, C.M. Stafford, X. Feng, M.T. Swihart, H. Lin, Unexpectedly strong size-sieving ability in carbonized polybenzimidazole for membrane H2/CO2 separation, ACS Appl. Mater. Interfaces 11 (50) (2019) 47365–47372.
- [13] L. Hu, V.T. Bui, A. Krishnamurthy, S. Fan, W. Guo, S. Pal, X. Chen, G. Zhang, Y. Ding, R.P. Singh, M. Lupion, H. Lin, Tailoring sub-3.3 Å ultramicropores in advanced carbon molecular sieve membranes for blue hydrogen production, Sci. Adv. 8 (10) (2022), eabl8160.
- [14] C.W. Jones, W.J. Koros, Carbon molecular sieve gas separation membranes-I. Preparation and characterization based on polyimide precursors, Carbon 32 (8) (1994) 1419–1425.
- [15] G.M. Iyer, C. Zhang, Precise hydrogen sieving by carbon molecular sieve membranes derived from solution-processable aromatic polyamides, ACS Mater. Lett. 5 (1) (2023) 243–248.
- [16] W. Ogieglo, T. Puspasari, A. Alabdulaaly, T.P. Nga Nguyen, Z. Lai, I. Pinnau, Gas separation performance and physical aging of tubular thin-film composite carbon molecular sieve membranes based on a polyimide of intrinsic microporosity precursor, J. Membr. Sci. 652 (2022), 120497.
- [17] Z. Wang, H. Ren, S. Zhang, F. Zhang, J. Jin, Carbon molecular sieve membranes derived from tröger's base-based microporous polyimide for gas separation, ChemSusChem 11 (5) (2018) 916–923.
- [18] K. Hazazi, Y. Wang, N.M.S. Bettahalli, X. Ma, Y. Xia, I. Pinnau, Catalytic arenenorbornene annulation (CANAL) ladder polymer derived carbon membranes with unparalleled hydrogen/carbon dioxide size-sieving capability, J. Membr. Sci. 654 (2022), 120548.
- [19] K. Hazazi, Y. Wang, B. Ghanem, X. Hu, T. Puspasari, C. Chen, Y. Han, I. Pinnau, Precise molecular sieving of ethylene from ethane using triptycene-derived submicroporous carbon membranes. Nat. Mater. 22 (10) (2023) 1218–1226.
- [20] D.-Y. Koh, B.A. McCool, H.W. Deckman, R.P. Lively, Reverse osmosis molecular differentiation of organic liquids using carbon molecular sieve membranes, Science 353 (6301) (2016) 804–807.
- [21] J. Liu, J. Goss, T. Calverley, G. Meyers, M.A. Thorseth, C.S. Todd, J. Kang, A. Denise, H. Clements, J. Klann, K. Mabe, L. Xu, M. Brayden, M. Martinez, Self-standing permselective CMS membrane from melt extruded PVDC, J. Membr. Sci. 615 (2020) 118554
- [22] L. Lei, F. Pan, A. Lindbråthen, X. Zhang, M. Hillestad, Y. Nie, L. Bai, X. He, M. D. Guiver, Carbon hollow fiber membranes for a molecular sieve with precise-cutoff ultramicropores for superior hydrogen separation, Nat. Commun. 12 (1) (2021) 268.

- [23] T. Araújo, M. Andrade, G. Bernardo, A. Mendes, Stable cellulose-based carbon molecular sieve membranes with very high selectivities, J. Membr. Sci. 641 (2022), 110852
- [24] T. Araújo, A.J. Parnell, G. Bernardo, A. Mendes, Cellulose-based carbon membranes for gas separations - unraveling structural parameters and surface chemistry for superior separation performance, Carbon 204 (2023) 398–410.
- [25] K.M. Steel, W.J. Koros, An investigation of the effects of pyrolysis parameters on gas separation properties of carbon materials, Carbon 43 (9) (2005) 1843–1856.
- [26] M. Kiyono, P.J. Williams, W.J. Koros, Effect of pyrolysis atmosphere on separation performance of carbon molecular sieve membranes, J. Membr. Sci. 359 (1) (2010) 2–10
- [27] M. Rungta, G.B. Wenz, C. Zhang, L. Xu, W. Qiu, J.S. Adams, W.J. Koros, Carbon molecular sieve structure development and membrane performance relationships, Carbon 115 (2017) 237–248.
- [28] N. Bhuwania, Y. Labreche, C.S.K. Achoundong, J. Baltazar, S.K. Burgess, S. Karwa, L. Xu, C.L. Henderson, P.J. Williams, W.J. Koros, Engineering substructure morphology of asymmetric carbon molecular sieve hollow fiber membranes, Carbon 76 (2014) 417–434.
- [29] C. Zhang, R. Kumar, W.J. Koros, Ultra-thin skin carbon hollow fiber membranes for sustainable molecular separations, AIChE J. 65 (8) (2019), e16611.
- [30] R.W. Baker, B.T. Low, Gas separation membrane materials: a perspective, Macromolecules 47 (20) (2014) 6999–7013.
- [31] Y. Cao, K. Zhang, C. Zhang, W.J. Koros, Carbon molecular sieve hollow fiber membranes derived from dip-coated precursor hollow fibers comprising nanoparticles, J. Membr. Sci. 649 (2022), 120279.
- [32] R. Kumar, C. Zhang, A.K. Itta, W.J. Koros, Highly permeable carbon molecular sieve membranes for efficient CO2/N2 separation at ambient and subambient temperatures, J. Membr. Sci. 583 (2019) 9–15.
- [33] J.E. Cadotte, F. Corp, Interfacially Synthesized Reverse Osmosis Membrane, 1981.
- [34] R.J. Petersen, Composite reverse osmosis and nanofiltration membranes, J. Membr. Sci. 83 (1) (1993) 81–150.
- [35] L. Zhao, W.S.W. Ho, Novel reverse osmosis membranes incorporated with a hydrophilic additive for seawater desalination, J. Membr. Sci. 455 (2014) 44–54.
- [36] D.F. Sanders, Z.P. Smith, R. Guo, L.M. Robeson, J.E. McGrath, D.R. Paul, B. D. Freeman, Energy-efficient polymeric gas separation membranes for a sustainable future: a review, Polymer 54 (18) (2013) 4729–4761.
- [37] G.M. Iyer, L. Liu, C. Zhang, Hydrocarbon separations by glassy polymer membranes, J. Polym. Sci. 58 (18) (2020) 2482–2517.

- [38] X. Ma, I. Pinnau, A novel intrinsically microporous ladder polymer and copolymers derived from 1,1',2,2'-tetrahydroxy-tetraphenylethylene for membrane-based gas separation, Polym. Chem. 7 (6) (2016) 1244–1248.
- [39] J. Park, K.E. Gaines, L.-C. Jheng, J.S. Riffle, S.J. Mecham, J.E. McGrath, H.B. Park, D.R. Paul, B.D. Freeman, Characterization and gas transport properties of UV-irradiated polydimethylsiloxane (PDMS)-containing polyimide copolymer membranes, Polymer 210 (2020), 122966.
- [40] M.R. Kosuri, W.J. Koros, Defect-free asymmetric hollow fiber membranes from Torlon®, a polyamide-imide polymer, for high-pressure CO2 separations, J. Membr. Sci. 320 (1) (2008) 65–72.
- [41] J. Vaughn, W.J. Koros, Effect of the amide bond diamine structure on the CO2, H2S, and CH4 transport properties of a series of novel 6FDA-based polyamide-imides for natural gas purification, Macromolecules 45 (17) (2012) 7036–7049.
- [42] H.-Y. Jang, J.R. Johnson, Y. Ma, R. Mathias, D.A. Bhandari, R.P. Lively, Torlon® hollow fiber membranes for organic solvent reverse osmosis separation of complex aromatic hydrocarbon mixtures, AIChE J. 65 (12) (2019), e16757.
- [43] D.Q. Vu, W.J. Koros, S.J. Miller, High pressure CO2/CH4 separation using carbon molecular sieve hollow fiber membranes, Ind. Eng. Chem. Res. 41 (3) (2002) 367–380
- [44] R.W. Baker, Membrane Technology and Applications, third ed., Wiley, West Sussex, England, UK, 2012.
- [45] O. Sanyal, S.S. Hays, N.E. León, Y.A. Guta, A.K. Itta, R.P. Lively, W.J. Koros, A self-consistent model for sorption and transport in polyimide-derived carbon molecular sieve gas separation membranes, Angew. Chem. Int. Ed. 59 (46) (2020) 20343–20347
- [46] K. Li, Q. Li, Z. Cai, Y. Weng, C. Ye, W. Ji, J. Li, B. Cheng, X. Ma, Microporosity effect of intrinsic microporous polyimide membranes on their helium enrichment performance after direct fluorination, J. Membr. Sci. 660 (2022), 120868.
- [47] H.A. Shawky, Performance of aromatic polyamide RO membranes synthesized by interfacial polycondensation process in a water–tetrahydrofuran system, J. Membr. Sci. 339 (1) (2009) 209–214.
- [48] W.J. Koros, G.K. Fleming, Membrane-based gas separation, J. Membr. Sci. 83 (1) (1993) 1–80.
- [49] J. Garrido, A. Linares-Solano, J.M. Martin-Martinez, M. Molina-Sabio, F. Rodriguez-Reinoso, R. Torregrosa, Use of nitrogen vs. carbon dioxide in the characterization of activated carbons, Langmuir 3 (1) (1987) 76–81.
- [50] H.D. White, C. Li, R.P. Lively, Tailoring the structure of carbon molecular sieves derived from an aromatic polyamide, Ind. Eng. Chem. Res. 61 (15) (2022) 5314–5323.